

# Realization of quantum anomalous Hall effect from a magnetic Weyl semimetal

Lukas Muechler,<sup>1</sup> Enke Liu,<sup>2,3</sup> Qiunan Xu,<sup>2</sup> Claudia Felser,<sup>2,\*</sup> and Yan Sun<sup>2,†</sup>

<sup>1</sup>*Department of Chemistry, Princeton University, Princeton, New Jersey 08544, USA*

<sup>2</sup>*Max Planck Institute for Chemical Physics of Solids, D-01187 Dresden, Germany*

<sup>3</sup>*Institute of Physics, Chinese Academy of Sciences, Beijing 100190, China*

(Dated: December 14, 2024)

The quantum anomalous Hall effect (QAHE) and magnetic Weyl semimetals (WSMs) are two topological states induced by intrinsic magnetic moments and spin-orbital coupling. The similarity between them suggests the possibility to archive the QAHE by dimensional confinement of a magnetic WSM along one direction. In this paper, we study the emergence of the QAHE in the two dimensional (2D) limit of magnetic WSMs due to finite size effects. We demonstrate the feasibility of this approach with both effective models and real materials. For that, we have chosen the layered magnetic WSM  $\text{Co}_3\text{Sn}_2\text{S}_2$  with both large anomalous Hall conductivity and anomalous Hall angle in the 3D bulk as our material candidate. In the 2D limit of  $\text{Co}_3\text{Sn}_2\text{S}_2$  we find two QAHE states. One is a semimetal with Chern number 6, and the other is an insulator with Chern number 3. The latter case has a band gap of 0.05 eV, which is much larger than that in magnetically doped topological insulators. Since intrinsic ferromagnets normally have a higher magnetic ordering temperature than dilute magnetic semiconductors, the QAHE obtained from WSMs should be stable up to a higher temperature, which is one of the most important parameters for further applications of the QAHE.

*Introduction.* The quantum anomalous Hall effect (QAHE) is the quantized version of anomalous Hall effect (AHE). In the QAHE, the transverse anomalous Hall conductance (AHC) is quantized in the unit of  $e^2/h$  and the longitudinal resistance reduces to zero [1–4]. Different from the ordinary AHE, the QAHE is topologically protected, which is characterized by a non-zero Chern number  $n$  and the presence of chiral edge states in the bulk band gap. Contrary to the quantum Hall effect with the formation of Landau levels induced by an external magnetic field, the QAHE originates from intrinsic magnetic moments and spin orbital coupling (SOC). Because of the absence of back scattering, the electron currents carried by the edge states are dissipationless [5]. Therefore, the realization of QAHE and the utilization of its chiral states may lead to a new generation of low energy consumption quantum electronic devices. It was proposed that, the integral of QAHE and superconductor via the proximity effect can generate the chiral Majorana fermions [6], which is thought to be a fundamental ingredient for the future of topological quantum computing.

The QAHE was firstly proposed in 1988 by F. D. M. Haldane via a theoretical model defined on the honeycomb lattice [4]. But because the special requirements of this model, the realization of QAHE in real materials took more than twenty years. Thanks to the developments of topological band theory and thin film growth techniques, the solution was solved in its counterpart of quantum spin Hall effect (QSHE) and topological insulators (TIs). The first QAHE was observed in the chromium-doped  $(\text{Bi,Sb})_2\text{Te}_3$ , where the TI gains the magnetic order through the Van Vleck paramagnetism [7, 8]. Based on the chiral edge states from Cr-doped  $(\text{Bi,Sb})_2\text{Te}_3$ , the chiral

Majorana Fermions (MFs) was recently observed in the heterostructure of QAHE and superconductor, which inspired strong enthusiasm for the comprehensive study of QAHE and MFs from both theory and experiments [9]. However, since the long distance between the magnetic impurities, it is a challenge to form the ferromagnetic order at high temperature in the magnetic-doped TI. So far the ferromagnetic Curie temperature is limited below 1 K. Together with the small band gap, the the QAHE in magnetic-doped TIs can only exist at an extremely low temperature ( $< 100$  mK), which strongly hinders its further studies and applications. Therefore, it is desirable to obtain new class of QAHE with large band gap and high Curie temperature based on a different approach. With this goal, much work has been devoted to the search of new QAHE materials based on different mechanisms, such as magnetic and antiferromagnetic semiconductors, heavy atom layers grown on magnetic substrate, transition metal oxides heterostructure, as well as absorption of atoms on quantum spin Hall insulators, etc [10–14]. However, there is still a large gap between the theoretical prediction and experimental realization, and much more research is to be done.

Very recently, another topological metallic states, the Weyl semimetal (WSM), was experimentally verified [15, 16], which have been viewed as a the QAHE in 3D version [17, 18]. Motivated by the progress in Weyl semimetals, we propose another efficient idea to obtain the QAHE. In WSM the conduction bands and valence bands linearly touch each other in 3D momentum space via the Weyl points, which behave as monopoles of the Berry curvatures with positive and negative chirality. According to symmetries, the WSMs can be classified into two classes, with and without time reversal symmetry. Since the Berry curvature is odd under time

reversal operation, the magnetic WSMs often host a strong AHE originated from the Weyl points. Since Weyl point can only be defined in 3D momentum space, it needs the translation symmetry in 3D. Therefore, the Weyl point can be removed by opening a band gap through the breaking of periodic boundary conditions along one direction. If the band order keeps the same as that in the 3d bulk state, it is possible to obtain the QAHE phase in the 2D limit of the magnetic WSMs. On the other hand, since the QAHE is a 2D system, magnetic WSMs with layered crystal structures are the preferred candidates for the realization of QAHE from the material point of view. In this work, we provide a proposal and one candidate material for archiving QAHE based on magnetic WSMs, which should be generalized to all other WSMs.

*Results.* To check the feasibility of this proposal, we firstly analyzed the 2D limit of the Weyl semimetal from a toy two band model,  $H = A(k_x\sigma(x) + k_y\sigma(y)) + M(k)\sigma_z$ , with  $M(k) = M_0 - M_1(k_x^2 + k_y^2 + k_z^2)$  [19]. As presented in Fig. 1(a), this model describes a magnetic WSM with one pair of Weyl points locating at  $\pm k_W$  of the  $k_z$ -axis and Fermi level ( $E_F$ ) just lies at the Weyl point. Owing to the Berry flux between this pair of Weyl points, the anomalous Hall conductivity obtains a peak value at  $E_F$  with  $\sigma_{AH} = (k_w/\pi)(e^2/h)$ , which is proportional to the separation of the Weyl points, see Fig. 1 (b) and (c) [19]. Breaking the periodic boundary condition in  $z$  direction, the Weyl points are removed by the opening of a band gap. Depending on the interaction strength between top and bottom sides of the film, the band order also varies as the changing of the thickness of the slab, resulting quantized jump of the AHC from zero to a finite number. With parameters setted in this work, the interactions from two surfaces remove the band inversion in the bulk state for the thickness of one and two unit cells. Increasing the slab thickness above three unit cells, the quantum confinement effect becomes weaker and band inversion appears for the subbands of the slab, which leads to quantized AHC and chiral edge state in the band gap, as shown in Fig. 1(d-f). Therefore, the mechanism for obtaining QAHE from magnetic WSM is principally allowed, but the realization of this conclusion from materials is still an open question.

So far, there are already many candidates for the magnetic WSMs from theoretical proposals, and some of them host strong AHE [17, 20–23]. Since the QAHE is a 2D insulator, so from the material point of view, the WSMs with large AHE, low charge carrier density, and layered lattice structure is preferred. In this work, we choose the quasi-2D material  $\text{Co}_3\text{Sn}_2\text{S}_2$  as the example to show the realization of QAHE from magnetic WSM.  $\text{Co}_3\text{Sn}_2\text{S}_2$  is a half metal with a rhombohedral lattice structure in the space group of R-3m (No. 166) [24–26]. The magnetic Co atoms are arranged in a Kagome lattice in  $x - y$  plane with magnetic moments along  $z$ .

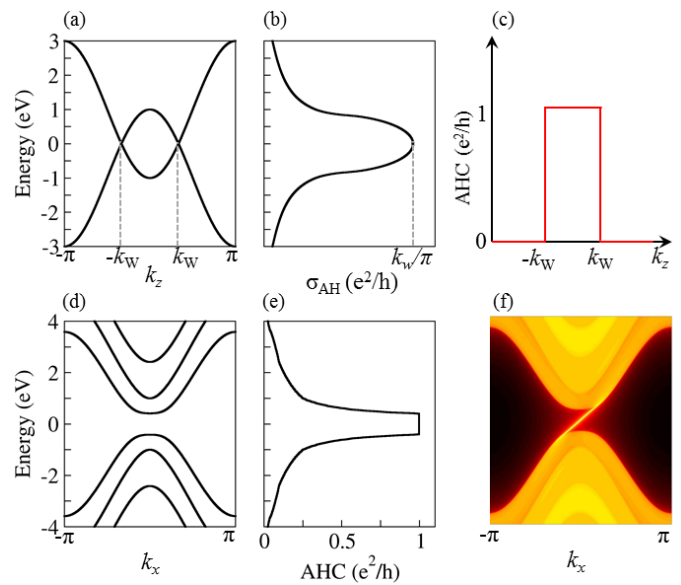


FIG. 1. (a) Energy dispersion along  $k_z$  and (b) energy dependent anomalous Hall conductivity for the WSM effective model. (c) Quantized anomalous Hall conductance (AHC) exists between one pair of Weyl points. (d) Energy dispersion for the slab from WSM effective model with thickness of three unit cells. (e) Anomalous Hall conductance (AHC) is quantized in the band gap of the film. (f) Energy dispersion of the edge states of the film. We have projected the  $k \cdot p$  model to a cubic lattice with lattice constant of 1 Å, and parameters of  $A=1.0$  eV Å,  $M_0=1$  eV, and  $M_1=1$  eV Å<sup>2</sup>

Putting the lattice in a hexagonal setting,  $\text{Co}_3\text{Sn}$  forms a quasi-2D layer and sandwich between S atoms. The quasi-2D layer  $\text{Co}_3\text{SnS}_2$  are connected by another atom Sn in the  $z$  direction.

Very recently, a large anomalous Hall conductivity up to 1100 S/cm was observed in  $\text{Co}_3\text{Sn}_2\text{S}_2$ , which is originated from the SOC induced node-line-like band anticrossings and Weyl points, see Fig. 2(b). Owing to the low charge carrier density, the anomalous Hall angle can reach up to 20%, which was never observed in other compounds. Compared to other magnetic WSMs, the Weyl points are quit close to  $E_F$ . So it offers a good opportunity to get an insulator state in 2D limit by the quantum confinement of size effect. Further more, because of the weak bonding connection between Sn and  $\text{Co}_3\text{SnS}_2$  layers, it should be easy to archive the 2D films by breaking this weak bonding. Therefore,  $\text{Co}_3\text{Sn}_2\text{S}_2$  provides a good platform for the interplay between QAHE and WSMs in real material.

There are two possible terminations for the cleaved  $\text{Co}_3\text{Sn}_2\text{S}_2$ , with Sn terminal and S terminal. The Co atoms form a Kagome lattice, with atom Sn lying in the center. Sandwiching Kagome lattice of  $\text{Co}_3\text{Sn}$  by two S layers, one obtains the minimal thickness for the S-terminated film of  $\text{Co}_3\text{SnS}_2$ , see Fig. 3(a). Further sandwiching the  $\text{Co}_3\text{SnS}_2$  by neighboring Sn

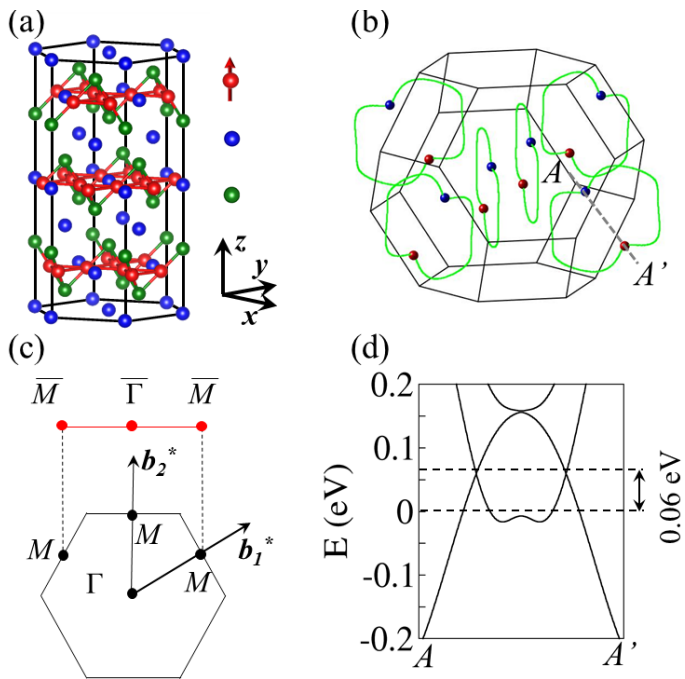


FIG. 2. (a) Lattice structure of  $\text{Co}_3\text{Sn}_2\text{S}_2$ . The spin polarization of the Co atom is along  $z$  direction. The primitive cell is marked by the dashed line. (b) Nodal lines and Weyl points distribution in BZ. Dots with red and blue colors represent opposite chirality of the Weyl points. (c) Two dimensional BZ of  $\text{Co}_3\text{Sn}_2\text{S}_2$  in  $k_x - k_y$  plane and its one dimensional projection. (d) Energy dispersion of  $\text{Co}_3\text{Sn}_2\text{S}_2$  along one pair of Weyl points. The labels for the  $k$  points are give in (b).

layers, we can get the other minimum thickness for the Sn-terminated film of  $\text{Co}_3\text{Sn}_3\text{S}_2$ . Via density functional theory (DFT) calculation [27, 28], we found that the preferred magnetic structure is the same as that in the bulk with magnetic polarization along  $z$ , which is also the requirement for obtaining QAHE in ferromagnet.

Without SOC, the  $\text{Co}_3\text{Sn}_2\text{S}_2$  film shows a semimetallic band structure. Different from the half-metallic state in the 3D bulk,  $\text{Co}_3\text{Sn}_2\text{S}_2$  film has both spin-up and spin-down channels cutting the Fermi level. Owing to the two mirror planes of  $M_x$  and  $M_y$ , both spin-up and spin-down channels form the linear band crossing around  $E_F$ , which are lying on the high symmetry lines of  $M - \Gamma$  and  $\Gamma - K$ , respectively, see Fig. 3(c). After the SOC is taken into consideration, the  $\text{SU}(2)$  symmetry is broken, leading to the gapping of the linear band crossings.

Moreover, viewing the energy dispersion in a larger energy window, we found that there is another linear band crossing on  $\Gamma - K$  with chemical potential shifting up around 0.6 eV and 4 electrons, which is just corresponding the minimum film for the Sn termination, however the system should be a semimetal from the perspective of transport. If just simply shifting the chemical potential to the upper linear band crossing

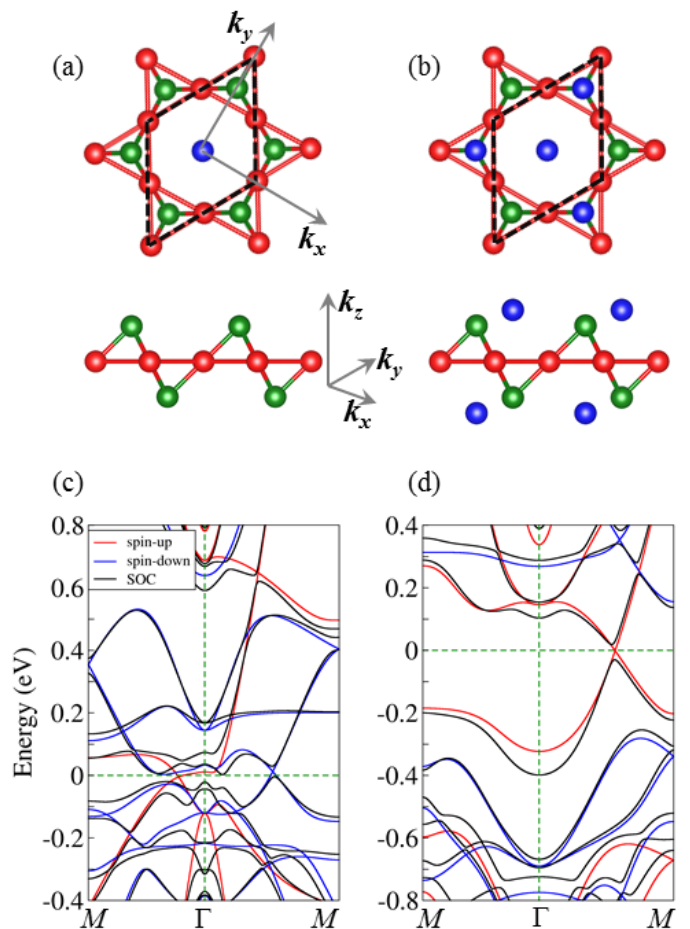


FIG. 3. (a, b) Lattice structure of  $\text{Co}_3\text{SnS}_2$  and  $\text{Co}_3\text{Sn}_3\text{S}_2$  film from the top (upper panel) and side (lower panel) view. (c, d) Energy dispersion for  $\text{Co}_3\text{SnS}_2$  and  $\text{Co}_3\text{Sn}_3\text{S}_2$  films with and without the inclusion of SOC.

point, see Fig. (c). However, the effect of Sn layers is not only offering extra electrons but also changes the dispersion of bands around  $E_F$ . As shown in Fig. 3 (d), after further sandwiching by Sn layers, the system forms an ideal semimetallic state with the Fermi surface only constructed by the linear crossing point. Similar to the situation in  $\text{Co}_3\text{SnS}_2$ , this linear band crossing is broken by SOC with opening a band gap. Compared to  $\text{Co}_3\text{SnS}_2$ , the Sn terminated slab has full band gap around 0.05 eV, which is much larger than that in magnetic impurity doped TIs.

To check the topological states, we have calculated the energy dependent AHC by integral of the Berry curvature in the whole BZ. The AHC for  $\text{Co}_3\text{SnS}_2$  can almost reach up to  $6 e^2/h$  at the charge neutral point. However, since  $\text{Co}_3\text{SnS}_2$  does not have a full band gap, its AHC changes sharply as varying the energy around  $E_F$ , and the maximum value only appears at an energy point, see Fig. 4(a). In contrast, the film of  $\text{Co}_3\text{Sn}_3\text{S}_2$  has a

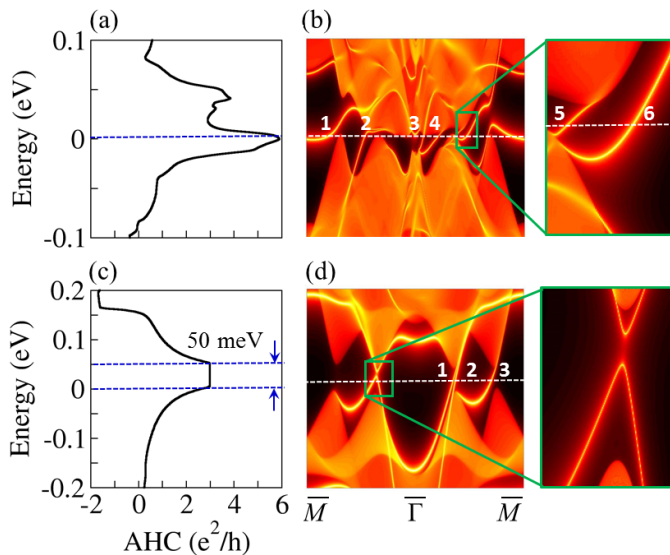


FIG. 4. (a, b) Energy dependent AHC for  $\text{Co}_3\text{SnS}_2$  film. The peak value with  $\text{AHC}=6 e^2/h$  appears at charge neutral point. (b) Energy dispersion of the edge states for  $\text{Co}_3\text{SnS}_2$  film. The local energy dispersion around edge states No.5 and No.6 are give on the right. (c) Quantized AHC ( $3 e^2/h$ ) appears in the band gap for  $\text{Co}_3\text{Sn}_3\text{S}_2$  film. (d) Edge states of  $\text{Co}_3\text{Sn}_3\text{S}_2$  film. The trivial dangling bond states is zoomed in on the right side.

constant quantized AHC in the energy window from  $E_F$  to  $E_F+50$  meV, as shown in Fig. 4 (c). So both the films of  $\text{Co}_3\text{SnS}_2$  and  $\text{Co}_3\text{Sn}_3\text{S}_2$  host nontrivial topological electronic structures with non-zero Chern number of 6 and 3, respectively.

A typical feature of the quantum anomalous Hall insulator and semimetal is the chiral edge state. To calculate the edge states, we have projected the Bloch wave functions into Wannier functions [29], and constructed the tight binding model Hamiltonian. The edge state was considered in an open boundary condition with the half-infinite one-dimensional model by using iterative Greens function method [30, 31]. The edge states of the energy dispersions for  $\text{Co}_3\text{SnS}_2$  and  $\text{Co}_3\text{Sn}_3\text{S}_2$  are given in Fig. 4(b) and (d), respectively. Due to the semimetallic property of  $\text{Co}_3\text{SnS}_2$ , there is not a general gap and the Fermi level cut the bulk valence bands and conduction bands slightly, which is consisted with the energy dependence of AHC. From the energy dispersion one can find six edge bands connecting the bulk conduction and valence states, and all of them have the same sign of Fermi velocity, which is just corresponding to the Chern number 6. Consisted with the Chern number 3 obtained from quantized AHC in  $\text{Co}_3\text{Sn}_3\text{S}_2$ , there are three topological protected edge states with positive Fermi velocity, see Fig. 4(d). Since the details of the edge states are strongly dependent on

the shapes of the edge terminations, one can also find the trivial states from the dangling bond. However, since the dangling bonds are not topologically protected, they don't connect the valence and conduction states from bulk, and should be easily annihilated by chemical engineering for the edge states.

*Summary.* In summary, we have theoretically studied the QAHE from the quantum confinement of the magnetic WSMs. Both the QAHE and magnetic WSMs are time reversal symmetry breaking systems, and the only symmetry needed for them is the periodic boundary condition. Since the WSM can be only defined in 3D momentum space, one method for the phase transition from WSM to QAHE is breaking the translational symmetry along one direction in WSM. Starting from the effective model, we have proved the feasibility of this idea. Since the QAHE is a 2D topological insulating state, the WSMs with strong AHE, low charge density, and layered lattice structure should be the preferred candidates. Considering these requirements for the real materials, we have focused on the layered magnetic WSM  $\text{Co}_3\text{Sn}_2\text{S}_2$  as the candidate for the realization of QAHE from WSMs. In the 2D limit of  $\text{Co}_3\text{Sn}_2\text{S}_2$ , we have found two possible QAHE states. One is semimetal states with Chern number 6, and the other one is insulator with Chern number 3 and band gap 0.05 eV. Compared to magnetic impurity doped TIs, the QAHE obtained from magnetic WSMs has larger energy band gap and high magnetic ordering temperature, which should provide a good possibility for the study and utilization of QAHE at high temperature.

This work was financially supported by the ERC Advanced Grant No. 291472 'Idea Heusler', ERC Advanced Grant No. 742068-TOPMAT and Deutsche Forschungsgemeinschaft DFG under SFB 1143. EL acknowledges supports from Alexander von Humboldt foundation of Germany for his Fellowship and from National Natural Science Foundation of China for his Excellent Young Scholarship (No. 51722106). LM would like to thank the MPI CPFS for its hospitality where part of the work was performed.

\* Claudia.Felser@cpfs.mpg.de

† ysun@cpfs.mpg.de

- [1] E. H. Hall, American Journal of Mathematics **2**, 287 (1879).
- [2] E. H. Hall, Philos. Mag. **12**, 157 (1881).
- [3] N. Nagaosa, J. Sinova, S. Onoda, A. H. MacDonald, and N. P. Ong, Rev. Mod. Phys. **82**, 1539 (2010).
- [4] F. D. M. Haldane, Phys. Rev. Lett. **61**, 2015 (1988).
- [5] B. I. Halperin, Phys. Rev. B **25**, 2185 (1982).
- [6] X.-L. Qi, T. L. Hughes, and S.-C. Zhang, Phys. Rev. B **82**, 184516 (2010).
- [7] R. Yu, W. Zhang, H.-J. Zhang, S.-C. Zhang, X. Dai, and Z. Fang, Science **329**, 61 (2010).

- [8] C.-Z. Chang, J. Zhang, X. Feng, J. Shen, Z. Zhang, M. Guo, L. Kang, Y. Ou, P. W. Wei, L.-L. Wang, Z.-Q. Ji, Y. Feng, S. Ji, X. Chen, J. Jia, X. Dai, Z. Fang, S.-C. Zhang, K. He, Y. W. Wang, L. Lu, X.-C. Ma, and Q.-K. X. Xue, *Science* **340**, 167 (2013).
- [9] Q. L. He, L. Pan, A. L. Stern, E. C. B. Burk, X. Che, G. Yin, J. Wang, B. Lian, Q. Zhou, E.-S. Choi, K. Murata, X. K. Kou, Z. Chen, T. Nie, Q. Shao, Y. Fan, S.-C. Zhang, K. Liu, J. Xia, and K. L. Wang, *Science* **357**, 294 (2017).
- [10] K. F. Garrity and D. Vanderbilt, *Phys. Rev. Lett.* **110**, 116802 (2013).
- [11] K. F. Garrity and D. Vanderbilt, *Phys. Rev. B* **90**, 121103(R) (2014).
- [12] K. F. G. Jianpeng Liu, Se Young Park and D. Vanderbilt, *Phys. Rev. Lett.* **117**, 257201 (2015).
- [13] L. Si, O. Janson, G. Li, Z. Zhong, L. Zhaoliang, G. Koster, and K. Held, *Phys. Rev. Lett.* **119**, 026402 (2017).
- [14] S.-C. Wu, B. Yan, and C. Felser, *EPL* **107**, 57006 (2014).
- [15] S.-Y. Xu, I. Belopolski, N. Alidoust, M. Neupane, G. Bian, C. Zhang, R. Sankar, G. Chang, Y. Zhujun, C.-C. Lee, H. Shin-Ming, H. Zheng, J. Ma, D. S. Sanchez, B. Wang, A. Bansil, F. Chou, P. P. Shibayev, H. Lin, S. Jia, and M. Z. Hasan, *Science* **349**, 613 (2015).
- [16] B. Q. Lv, H. M. Weng, B. B. Fu, X. P. Wang, H. Miao, J. Ma, P. Richard, X. C. Huang, L. X. Zhao, G. F. Chen, Z. Fang, X. Dai, T. Qian, and H. Ding, *Phys. Rev. X* **5**, 031013 (2015).
- [17] X. G. Wan, A. M. Turner, A. Vishwanath, and S. Y. Savrasov, *Phys. Rev. B* **83**, 205101 (2011).
- [18] A. A. Burkov and L. Balents, *Phys. Rev. Lett.* **107**, 127205 (2011).
- [19] H.-Z. Lu, S.-B. Z. Zhang, and S.-Q. Shen, *Phys. Rev. B* **92**, 045203 (2015).
- [20] G. Xu, H. Weng, Z. Wang, X. Dai, and Z. Fang, *Phys. Rev. Lett.* **107**, 186806 (2011).
- [21] Z. W. Wang, M. G. Vergniory, S. Kushwaha, M. Hirschberger, and E. V. Chulkov, *Physical Review Letters* **117**, 236401 (2016).
- [22] T.-R. Chang, G. Chang, C.-C. Lee, S.-M. Huang, B. Wang, G. Bian, H. Zheng, D. S. Sanchez, I. Belopolski, N. Alidoust, M. Neupane, A. Bansil, H.-T. Jeng, S.-Y. Xu, H. Lin, and M. Z. Hasan, *Nat. Commun.* **7**, 1 (2016).
- [23] J. Kubler and C. Felser, *EPL* **114**, 4 (2016).
- [24] R. Wehrich, I. Anusca, and M. Zabel, *Z. Anorg. Allg. Chem.* **631**, 1463 (2005).
- [25] P. Vaqueiro and G. G. Sobany, *Solid State Sci.* **11**, 513 (2009).
- [26] W. Schnelle, A. L. Jasper, H. Rosner, F. M. Schappacher, R. Pttgen, F. Pielhofer, and R. Wehrich, *Phys. Rev. B* **88**, 144404 (2013).
- [27] G. Kresse and J. Furthmüller, *Phys. Rev. B* **54**, 11169 (1996).
- [28] J. P. Perdew, K. Burke, and M. Ernzerhof, *Phys. Rev. Lett.* **77**, 3865 (1996).
- [29] A. A. Mostofi, J. R. Yates, Y.-S. Lee, I. Souza, D. Vanderbilt, and N. Marzari, *Comput. Phys. Commun.* **178**, 685 (2008).
- [30] M. P. L. Sancho, J. M. L. Sancho, and J. Rubio, *Phys. F: Met. Phys* **14** (1984).
- [31] M. P. L. Sancho, J. M. L. Sancho, and J. Rubio, *Phys. F: Met. Phys* **15** (1985).